Directed network topologies of smart grain sensors

David M. Walker and Antoinette Tordesillas*
Department of Mathematics and Statistics, University of Melbourne, Parkville, VIC 3010 Australia

Tomomichi Nakamura
Graduate School of Simulation Studies, University of Hyogo, 7-1-28 Minatojima-minamimachi, Chuo-ku, Kobe, Hyogo 650-0047, Japan

Toshihiro Tanizawa
Kochi National College of Technology, Monobe-Otsu 200-1, Nankoku, Kochi 783-8508, Japan
(Received 22 November 2012; revised manuscript received 14 February 2013; published 11 March 2013)

We employ a recent technique for building complex networks from time series data to construct a directed network embodying time structure to collate the predictive properties of individual granular sensors in a series of biaxial compression tests. For each grain, we reconstruct a static predictive model. This combines a subset selection algorithm and an information theory fitting criterion that selects which other grains in the assembly are best placed to predict a given grain's local stress throughout loading history. The local stress of a grain at each time step is summarized by the magnitude of its particle load vector. A directed network is constructed by representing each grain as a node, and assigning an in-link to a grain from another grain if the latter is selected within the best predictive model of the first grain. The grains with atypically large out-degree are thus the most responsible for predicting the stress history of the other grains: These turn out to be only a few grains which reside inside shear bands. Moreover, these "smart grains" prove to be strongly linked to the mechanism of force chain buckling and intermittent rattler events. That only a small number of grain sensors situated in the shear band are required to accurately capture the rheological response of all other grains in the assembly underlines the crucial importance of nonlocal interactions, espoused by extended continuum theories which posit nonlocal evolution laws. Findings here cast the spotlight on two specific mechanisms as being key to the formulation of robust evolution laws in deforming granular materials under compression and shear: the long held mechanism for energy dissipation of force chain buckling and the sudden switch in roles that a rattler plays as it enters in and out of force chains.

DOI: 10.1103/PhysRevE.87.032203 PACS number(s): 81.05.Rm

I. INTRODUCTION

What if some kind of smart grain sensor could be designed which, to all intents and purposes, had the same rheological response as the grains themselves but was capable of recording and transmitting useful kinematic or force information to experimentalists? Two trends in sensor technologies suggest that the existence of such sensors is close to, if not already, a reality: miniaturization to tens of nanometers and an ever increasing range of sensing capabilities including measurements of pressure, inertial forces, magnetic fields, chemical structure, and species [1]. Armed with a network of such sensors a researcher could perhaps seed, or salt, a fault gouge, foundations of a building, runway tarmac, etc., to monitor the activity and, based on the transmitted information, have real-time monitoring of the likely response of the fault, building foundations, and so on. Despite great advancements in science and industry of sensor technology, notably microelectromechanical sensors (MEMs) which include gyroscopes, accelerometers, and magnetometers, we are some way away from granular microelectromechanical sensors (gMEMs). We can, however, turn to virtual particle simulations using the discrete element method (DEM) and regard the grains as being their own sensor network. If we do this, we can then ask what information should the sensors sense, how many sensors do we need to tell us something useful, what extent of the material should the sensor network encompass, and of course, how do we process and summarize such information?

Perhaps the most pertinent question above is how can data collected by yet-to-be-realized sensors be of greatest utility to material characterization and modeling, in particular predictive continuum modeling of granular matter. To develop robust predictive continuum models for soil, rocks, powder, and other forms of granular matter, we need information at the grain scale as has been recognized for over a century [2]. The advance of DEM has been an invaluable and often the only source of grain scale information to date (e.g., [3,4]); however, high-resolution experimental data from soil micromechanics are accumulating steadily (e.g., [5–12]). Irrespective of the source of grain scale information, virtual or experimental, the development of robust and tractable continuum models requires the modeler to make sense of the voluminous data and distill these down to a few fundamental rules that can reproduce the emergent, self-organized behavior observed in reality. To achieve this objective comprehensively, the modeler must account for two aspects of granular behavior under load. The first is a structural aspect from local interactions: here at the physical grain to grain contacts. The second is a hidden dynamical aspect from nonlocal interactions: grains, near and far, interact with and influence a grain through collective behavior, and arguably the most striking example of this lies in force transmission, through so-called force chains. Clearly, these two aspects are intertwined. Therefore, a prevailing

*atordesi@unimelb.edu.au

challenge for modelers of granular systems lies in finding strategies that can treat these aspects not independently, but seamlessly in a single unified framework.

In this study, we propose a strategy for the analysis and characterization of force transmission. Though we demonstrate this strategy for quasistatically loaded dense assemblies of grains which do not break and are cohesionless, it has potential applications in the study of a wider range of granular materials. Indeed while systems in the presence of binders and particle breakage are examples farther away from the systems we envisage here to be inhabited by the aforementioned gMEMs, there are nonetheless common attributes in the way forces are transmitted in a broad gamut of granular and, more broadly, soft matter (e.g., polymers, colloids, gels, and foams); see, for example, [13–21]. The formation of a highly heterogeneous, ramified, and intermittent force network has been observed to be a fundamental process across a range of loading conditions and particle properties. For example, in 2D and 3D experiments [5,6,9,22–28] and also 2D and 3D simulations [10–12,29–31], force chains and their failure have been tied to energy dissipation and core processes of grain rearrangements.

The specific objective of this paper is to consider the possibility of gMEMs, and to demonstrate a way of processing and summarizing the observed information on force transmission to improve our understanding of the highly interdependent local and nonlocal grain interactions occurring in deforming cohesionless, dense granular materials. Particular attention will be paid to the complex phenomena of self-organized structures of grains in a dual network of force chains and confining weak neighbors, and the related emergence of shear bands when such load-bearing chains fail. We use a combination of time series modeling, information theory processing, and complex network analysis to develop an abstract directed network which encompasses the essential linear relationships between the force response of individual grains. We find a special subset of these grains—those which have higher out-degree than in-degree in the network—to be intimately related to the mechanism of confined buckling of force chains and give these grains the specific moniker of "smart sensors" in contrast to the general future smart gMEMs we have envisaged above.

The remainder of this paper is organized as follows. In Sec. II, we briefly describe the suite of DEM tests examined, the data used, and our method of obtaining a directed complex network from models of the time series data. To consolidate ideas, we apply the methods to a small subset of grains in Sec. III. In Sec. IV, we present the results of applying our methods to each of the DEM tests. We close the paper in Sec. V by discussing the relevance of our findings in the context of continuum constitutive modeling.

II. METHODOLOGY

We develop our ideas using synthetic data from DEM simulations. Using output from DEM simulations affords us the opportunity to explore the possibilities that future sensors measuring grain stresses may provide. We also restrict our investigation to a suite of DEM simulations previously studied where the (virtual) rheology is more fully, if not completely, understood. Consequently, any perspective from the proposed sensor analysis can be properly assessed and appreciated.

A. DEM simulation

The data analyzed are taken from a series of biaxial compression tests from an initially isotropic state, verified by examining distributions of contact angles within the initial packing. The simulations are 2D although this is achieved by constraining assemblies of spherical grains to move in a plane (see, e.g., [32–34]). The four tests differ from each other with respect to boundary loading conditions or value of rolling friction. Two of the tests are subject to constant volume (or area), referred to by the label CV; the remaining two are subject to constant confining pressure at the lateral walls.

The interaction between a grain at contacts with the other grains and with the walls is modeled by a set of contact laws which describe resistances to relative motion through various combinations of a linear spring, a dashpot, and a friction slider. Normal and tangential resistive forces, as well as a moment (rolling resistance), act at each contact, in accordance with [29]. The contact moment is introduced to account for the effect of grain shape, e.g., resistance to relative rotations due to grain interlocking [35]. This modification to the classical DEM model of [36] has been adopted in numerous simulations of granular processes in order to control the relative rotations of grains at contacts and achieve more realistic rotations and stress predictions (e.g., [37]). Each of the four tests are distinguished by the coefficient of rolling friction $\mu^r = 0.02$ or 0.2. The vertical walls in all the tests are frictionless, so that grains can slide and roll along them without any resistance; otherwise, all other material properties are identical to those of the grains. The top and bottom walls are assumed to have the same material properties as the grains. Table I provides a summary of the simulation, material, and contact model parameters

TABLE I. DEM parameters and material properties for planar deformation of an assembly of spheres constrained to move in a plane. The initial packing was isotropic confirmed by examining distributions of the direction of branch vectors. Parameters and sectional properties below are per unit depth (into the page).

Parameter	Value
Applied strain rate $\dot{\epsilon}_{yy}$	-8×10^{-3}/s
Confining pressure σ_{xx} (when applicable)	7.035×10^{2} N/m
Time step increment	6.81×10^{-7} s
Initial height:width ratio	1.08:1
Number of grains	5098
Grain density	2.65×10^{3} kg/m^3
Smallest radius	0.76×10^{-3} m
Largest radius	1.52×10^{-3} m
Average radius (uniform distribution)	1.14×10^{-3} m
Initial packing density	0.858
Intergrain friction μ	0.7
Grain-wall friction μ (top, bottom)	0.7
Grain-wall friction μ (sides)	0.0
Rolling friction μ^r	0.02 or 0.2
Normal spring stiffness k^n	1.05×10^{5} N/m
Tangential spring stiffness k^t	5.25×10^{4} N/m
Rotational spring stiffness k^r	6.835×10^{-2} N m/rad

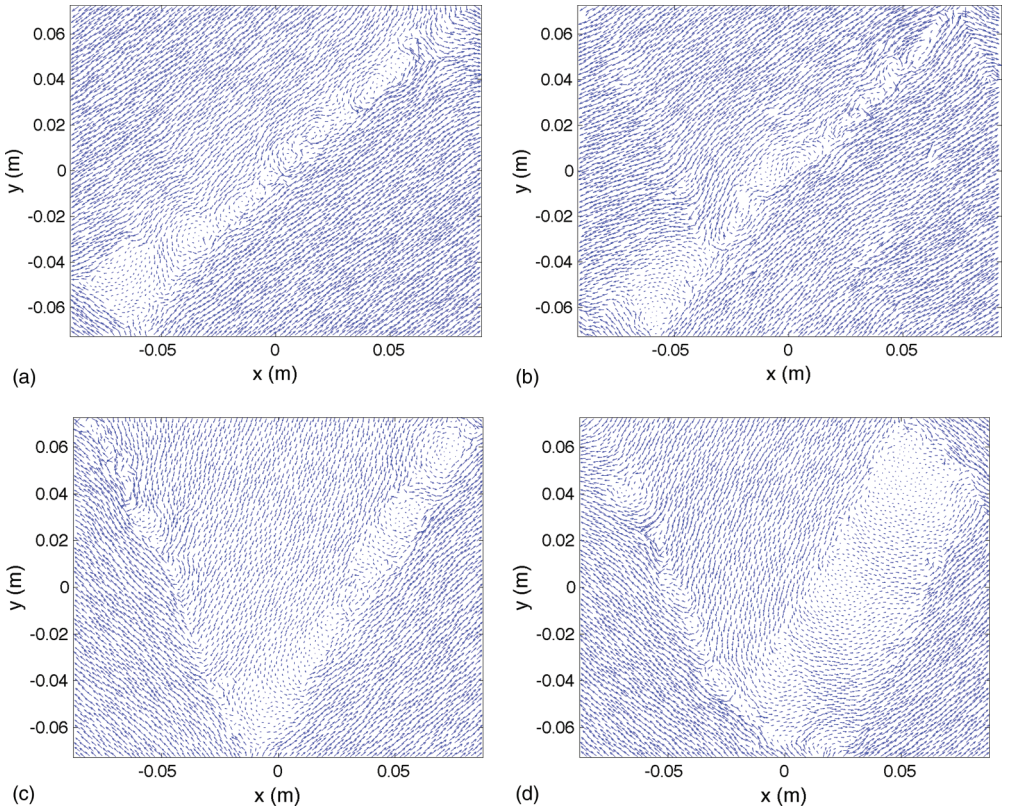

FIG. 1. (Color online) Displacement field for the four tests across strain increments in the large strain failure regime after peak stress ratio. Constant confining pressure (a) $\mu^r = 0.02$, (b) $\mu^r = 0.2$ for axial strain increment 0.0115. Constant volume (c) $\mu^r = 0.02$, (d) $\mu^r = 0.2$ for axial strain increment 0.0107.

used (i.e., polydisperse grain distribution, friction coefficients, spring model stiffness coefficients, etc.). The initial size of the container satisfies a height-to-width ratio of 1.08:1.0 and in the constant confining pressure test with $\mu^r = 0.02$ after one observed strain state the container is approximately 15.3 cm × 16.6 cm. Additional details relating to sample preparation, as well as choices of integration time steps and damping terms to achieve quasistatic conditions, are fully discussed elsewhere [33]. In all four samples, the development of a persistent strain localization (i.e., shear banding) is captured. To aid visualization and for comparison purposes, the zones of localization in each sample are presented in Fig. 1 as seen from the grain displacement field.

As mentioned, each of these samples belongs to a class of DEM simulations that has been studied in detail using a variety of methodologies. The mechanical response of the samples exhibits the expected trends for dense granular assemblies [33]. Techniques from micromechanics, in particular micropolar nonaffine deformation measures, describe temporally and spatially the areas of local grain rearrangements responsible for energy release and dissipation within the systems throughout loading [33,38]. These areas have been demonstrated to coincide with the structural failure of force chain columns by buckling [34,39].

More recently, the methods of complex network theory have been used to characterize the fabric, force anisotropy, and emergent behavior through the evolution of contact network representations of the grains. These networks whereby a network node represents a grain and a network link connects two nodes if the corresponding grains are in physical contact highlight the role of formation and breaking of links (contacts) as well as larger connected network structures in the deforming material [40–42]. Networks with links based on similarity of grain kinematic evolution across strain increments have also been constructed and analyzed to reveal other novel features of the rheology of systems from this class of simulations, as well as from experimental tests on sand [28,43].

While these network methods have proven to be useful, they are somewhat limited by their lack of a system wide perspective. For instance, in [28], the temporal history of the sand specimen's behavior under load was not accounted for, as information from each individual observation strain state was examined separately and independently of system behavior at other states. On the other hand, the work in [43] did consider temporal information, but did not consider how grain interactions at one state influence those at another state of the loading history. Here we take the first steps towards such an analysis, in particular, one which better accounts for the interdependence of grain behavior across the temporal dimension—beyond similarity of macroscopic response across different strain states. Specifically, here we propose to analyze the samples through the lens of complex networks with the added information on relationships between grain scale properties as they evolve temporally across many strain increments, or even the entire loading history. We do this by constructing models of the relationship between time series of grain properties, in particular grain stresses, and collating the information contained in all of these models as a

directed complex network. We find that the basic properties of these networks reveal which grains have the richest rheological information throughout the loading history, thus enabling us to relate them to known mesoscopic mechanisms governing energy storage and dissipation in deforming granular materials.

B. Particle load vector time series

Consider each grain to be its own internal sensor (gMEMs) capable of measuring its internal stresses caused by contact with other grains. This quantity can be found by calculating what is referred to as a particle load vector. Mathematically, the stress tensor provides a measure of the force anisotropy within an assembly of granular particles. We define (for a circular grain A with k contacting circular grains) the local force moment tensor as

$$\hat{\sigma}_{ij} = \sum_{c=1}^{k} n_i^{Ac} f_j^{Ac} (R^{Ac} + R^{Bc}), \quad i,j = 1,2. \tag{1}$$

Here, f_j^{Ac} is the jth component of the contact force between grain A and a contacting grain B, n_i^{Ac} is the component of the unit branch vector from grain A to the contact with grain B, R^{Ac} and R^{Bc} are the radii of the two contacting grains, and the sum is taken over all k contacts of grain A. Incidentally, the number of contacts k is the degree of the induced node of grain A in a contact network representation of the fabric of the material (cf. coordination number). The matrix $\hat{\sigma}_{ij}$ and its eigenvectors and eigenvalues are calculated. The largest eigenvalue and its associated eigenvector define the particle load vector. Its magnitude is the stress used to construct our grain sensor load time series for each strain state of the deformation. As an aside, if we were to sum the contributions of (1) for each grain in the assembly and normalize by the area of the assembly to get a global force moment tensor Σ_{ij}, then the eigenvalues of this matrix (say, $\sigma_1 \leqslant \sigma_2$) give the pressure $P = \frac{1}{2}(\sigma_1 + \sigma_2)$ and the shear stress $\tau = \frac{1}{2}(\sigma_2 - \sigma_1)$. For each axial strain state of the deformation we normalize each local particle load time series value by the total sum of values across the assembly. Thus we obtain, for each of the 5098 grains in the assembly, a time series of length 299 (i.e., the number of axial strain states observed). Typical time series for three grains are shown in Fig. 2. These are examples of the time series we build models for, as explained below.

C. Building a static predictive model

A complete and accurate model of the relationships between the properties of grains which interact locally yet exhibit emergent collective behavior is likely to involve complex nonlinearities. However, prominent relationships and interactions may still be uncovered by considering appropriate linear models. Indeed, even if the underlying process of observed time series data has a nonlinear source, often useful information and essential features can be extracted using the linear tool of Fourier series through a power spectrum analysis. For example, modeling the buckling of force chain structures in granular materials using approximating Fourier series models identified a characteristic length scale of shear bands to be around eight grains wide [44]. A combined structural mechanics and a micropolar continuum analysis of

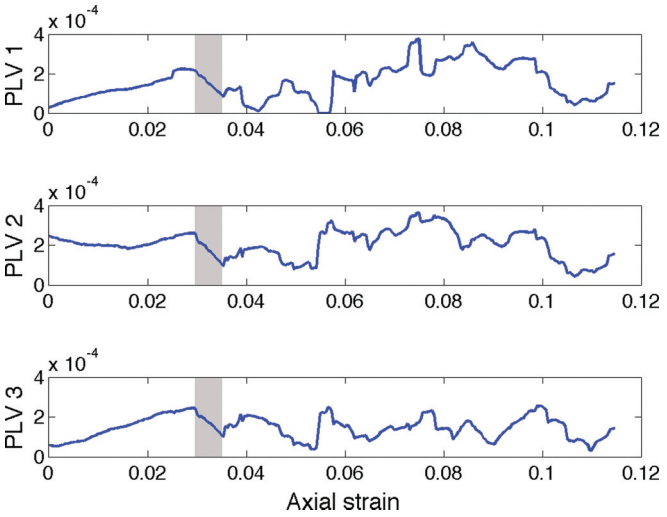

FIG. 2. (Color online) The time series of particle load vector magnitude for the force chain cluster shown in Fig. 3. The shaded sections highlight the start and end of the strain increment where the clusters were drawn. We search for linear relationships between these time series. For example, the time series of PLV 1 could be predicted by a linear combination of the time series of PLV 2 and PLV 3.

a confined elastic-plastic buckling of a 3-particle force chain also revealed that, for a given strain state, the normal stresses in this mesoscopic cluster are linearly related. Thus even in these profoundly nonlinear processes, some linear relations manifest among stresses at distinct *static equilibrium states* of the sample's loading history.

Here we build a class of linear models for each particle load time series, inspired by the reduced autoregressive (RAR) model fitting methods developed for detecting periodicity in (possibly) nonlinear data [45]. The method involves the use of an information theory criterion, namely description length, to select which linear combination of past values of a time series is best able to fit the current value of the time series without overfitting the data. The use of description length in this way has been extended to nonlinear combinations of past values of the time series with success [46].

Our use of RAR is similar in spirit to the method of principal orthogonal decomposition, or principal components analysis (PCA). In PCA, data are projected to a smaller subspace which contains most of the information contained in the data with the contribution of the "ignored" dimensions attributed to noise. The size of the smaller subspace, or number of principal components, is determined by examining the eigenvalues of a covariance matrix constructed from the data. The selection of the number of principal components is often a subjective choice, dependent on the skill and experience of the researcher. The RAR modeling approach we follow here also attempts to determine a smaller subspace in which to describe the data; however, the incorporation of the information theory description length introduces a more objective framework to decide what constitutes the "best" subspace.

The description length of a model of observed data consists of a term capturing how well the model fits the data, and terms which penalize for the number of parameters needed for the model to achieve a prescribed accuracy. Specifically, an

approximation to description length takes the form

$$DL(k) = N \ln(\mathbf{e}^T \mathbf{e}/N) + k\left(\frac{1}{2} + \ln \gamma\right) - \sum_{j=1}^{k} \ln \hat{\delta}_j, \qquad (2)$$

where N is the length of the time series to be fitted and $\mathbf{e}$ are the fitting errors. The latter two terms comprise the penalty for model size with k being the number of parameters and $\hat{\delta}_j$ the accuracy with which the parameters must be specified. These $\hat{\delta}$'s are found by solving a nonlinear optimization problem setup using the Hessian of the likelihood function of the data and is explained in great detail elsewhere, e.g., [45,47]. The factor γ is just a constant and typically fixed to be $\gamma = 32$ [47].

In [45,48,49], RAR models are reconstructed using a scalar time series. In our case, we employ that methodology to reconstruct for each particle load time series a static predictive model which is a linear combination of a subset of the other grains time series. Specifically, we predict the particle load vector magnitude of grain i at time t as

$$x_i(t) = \lambda_0 + \sum_{c \in S(i)} \lambda_c x_c(t), \qquad (3)$$

where the λ_i are parameters estimated using least squares, and $S(i)$ is the subset of grains, not including grain i itself, which have been selected as having the best history of particle load values to predict $x_i(t)$ with respect to description length in (2) and given a linear model class of the form in (3). This subset is determined in an iterative growing and culling algorithm established by [46]. The parameter λ_0 is also considered part of the subset for selection and so may or may not be present in the model. Note that selecting the optimal subset from a large dictionary of basis functions is typically an NP-hard problem which usually has to be solved by heuristic methods [46]. The models obtained by selection algorithms can offer near-optimal models. The selection algorithm we use has proven to be effective in modeling nonlinear dynamics [46,50].

Our procedure is to find the best subset of particle load histories which best predicts a given grain's load history. The best model is taken to be that model which minimizes the description length. We do this for all grains in the assembly, and summarize the information of these best models using a directed network as described below in a fashion similar to and inspired by [48,49].

D. Directed network construction

In [48,49], weighted directed networks embodying the time structure of scalar time series were constructed. By encapsulating the time structure present in a time series, these networks extended and complemented the idea of studying nonlinear dynamics using a complex network representation constructed by considering closeness of pseudocycle sections of the time series or distance in phase space, etc. [51–54]. Once the nodes are defined in pseudocycle networks (nodes are individual pseudo-cycles) or phase space networks (nodes are reconstructed phase space points), all information regarding time evolution is suppressed and not exploited. By contrast, in the approach of [48,49], directed networks were developed by first assigning a node to each scalar value of the time series and then adding weighted directed links if earlier values of the time series (nodes) appeared in the best RAR predictive model. Thus the time structure in terms of predictability of the time series is encoded into the direction of the links of the networks. The links were further assigned weights based on a transformation of the coefficients of the fitted RAR models. Our approach using the static predictive models of the previous section and multivariate time series differs slightly in a way which we now explain.

The nodes of our network represent each grain (i.e., each of the multivariate time series). We connect a directed link *in* to node i from other grain nodes if that grain is selected in the modeling using (2) and (3). If a grain j is used in (3) then clearly that grain's node j has an *out* link. We ignore the λ_0 term regardless of its being included in the best models as it does not represent a grain. In future work, it might be interesting to create an *über* node representing this constant term. We do not include the transformation of the coefficients to obtain weights for the links as in [48,49] despite its being straightforward to do so. Here, we are more interested in the unweighted structural topology of the resulting directed networks and reserve the addition of the weights to a future investigation which will also consider more general feedback predictive models than the static linear ones described in (3). Accordingly, of interest is the in-degree of a grain (i.e., the number of other grains deemed best to predict its particle load behavior) and the out-degree of a grain (i.e., the number of grain models it appears in). Important quantities of note are thus the distribution of in-degree, the distribution of out-degree, and any grains with atypically large out-degree.

III. A SIMPLE EXAMPLE

We first demonstrate our strategy for a small granular cluster to render transparent and make our ideas more concrete and understandable. Consider a simple example of a particle load vector time series of the cluster of grains in Fig. 3, which is taken from one of the constant confining pressure tests with $\mu^r = 0.02$. This cluster depicts the arrangement of a three-grain force chain (IDs 1, 2, and 3) and its confining neighbors (IDs 4–11). The cluster is shown for two axial strain states where the first Fig. 3(a) shows the force chain prior to failure by buckling and Fig. 3(b) shows the grains after the force chain has failed by buckling. This force chain has been previously identified as being the trigger buckling event precipitating failure in the material. The particle load time series of Fig. 2 correspond to the grains with IDs 1, 2, and 3 in this cluster. The gray shaded area indicates the strain increment where the clusters in Fig. 3 are shown.

For each grain in this cluster, we build a static predictive model of the form of (3) using the other particle load time series of the cluster and use (2) to evaluate the best subset of these for prediction. A directed graph is constructed with adjacency matrix elements $a_{ij} = 1$ if grain j belongs in the best subset of grains to predict the particle load time series of grain i. The adjacency matrix obtained by this procedure is represented in Fig. 4 where nodes are labeled by grain ID and the arrows show the in- and out-links in the network.

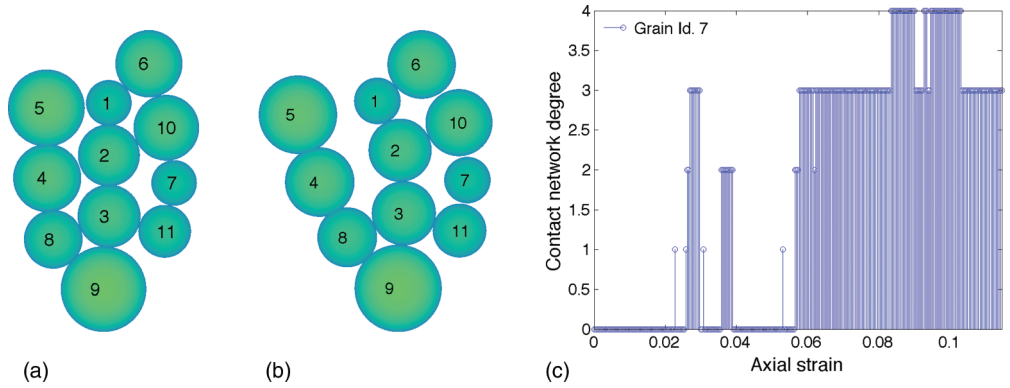

FIG. 3. (Color online) A cluster of grains comprising a force chain and its confining neighbors at two strain states (a) 0.0296, (b) 0.035 taken from the $\mu^r = 0.02$ constant confining pressure compression test. The buckling of this force chain has previously been identified as the "trigger" buckling event that precipitated the failure of the material, i.e., the first force chain buckling that initiated the formation of the persistent shear band. The cluster depicted in (a) is prior to this buckling event and in (b) is many axial strain stages after buckling. The grain ID is shown as an *aide memoire* for Fig. 4. (c) The contact network degree of grain ID 7 demonstrating the changing contact topology a grain can experience throughout deformation.

IV. RESULTS

Having consolidated how the idea works on a small subset of grains, we can now study the entire assembly in each of the four test systems. For the size of our systems (i.e., 5098 grains/nodes) it becomes difficult to visualize the directed networks in the same manner as Fig. 4. We must instead rely on summary statistics although it is useful and informative to view the nonzero entries of the directed network adjacency matrix. In Fig. 5 we show the adjacency matrices obtained for all four test systems which summarizes the grain membership of each static predictive linear model as determined by description length. In these figures, each row and column corresponds to a grain identification label. If we scan along a given row (i.e., we select a grain), then the dots (i.e., nonzero entries) represent the grains which have been selected to have the best linear combination of particle load vector histories to predict the history of the grain in question. A row sum thus represents the in-degree of a grain and corresponds to the number of other grains required to best predict that grain's history. On the other hand, the column sum represents how many times a given grain appears in the best models of other grains. As observed in Fig. 5, a distinct structure to these adjacency matrices manifests for each test. The appearance of bold vertical linelike columns suggests that the particle load vector histories of some grains are more representative of the response of other grains throughout loading than others.

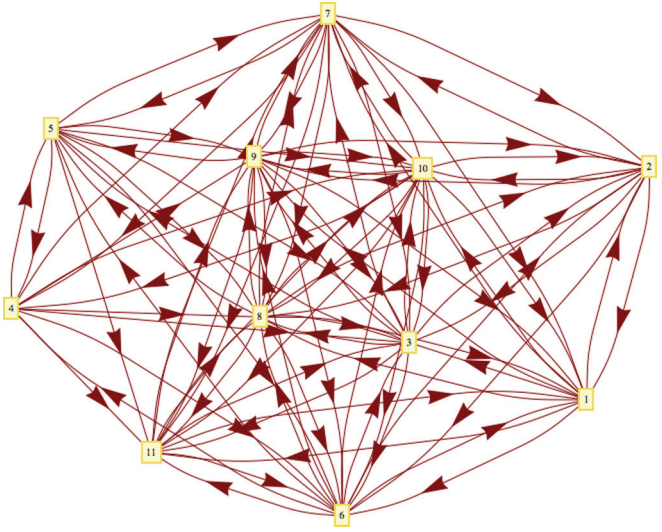

FIG. 4. (Color online) The directed network summarizing the predictive models of the particle load vector time series. Nodes are labeled by grain ID. An in-link means the originating grain is used in a model of a destination grain. An out-link means that grain is present in a model of another grain. Note that here only the grains in the trigger cluster form the set of grains for which the subset of grains in model (3) are selected.

The in-degree and out-degree distributions help clarify this situation further. In Fig. 6, we show the empirical distribution of grain in-degrees for all tests. Across the tests, there is remarkable consistency in these distributions. Regardless of test, it appears that the typical model size (i.e., number of other grains deemed best to predict a given grain's particle load vector history) is around 10–12 (the mean of the empirical in-degree distribution) and at most 30. Hence, if we wanted to salt a granular material with smart gMEMs for real-time monitoring, we may only need 10 sensors for around 5000 grains (i.e., the size of our test systems). Furthermore, the consistency in the results for all the tests, keeping in mind these differ in material properties as well as loading conditions, suggests this finding may be generic to dense granular materials. The *same* set of 10–12 sensors would not lead to the best set of relationships describing the behavior of all grains. A larger set of grain sensors is likely necessary to obtain an improved balance of sensor numbers to RAR relationship accuracy for the entire assembly. A guide to such a number can be found by examining the out-degree distribution.

In Fig. 7, we plot the empirical distribution of grain out-degree for all tests. This distribution is conveniently viewed on a log-log scale: Despite showing hints of power law behavior, any maximum likelihood fit does not pass a rigorous significance test. Nevertheless, whatever the best mathematical explanation for the distribution might be, we once again observe remarkable consistency across the different

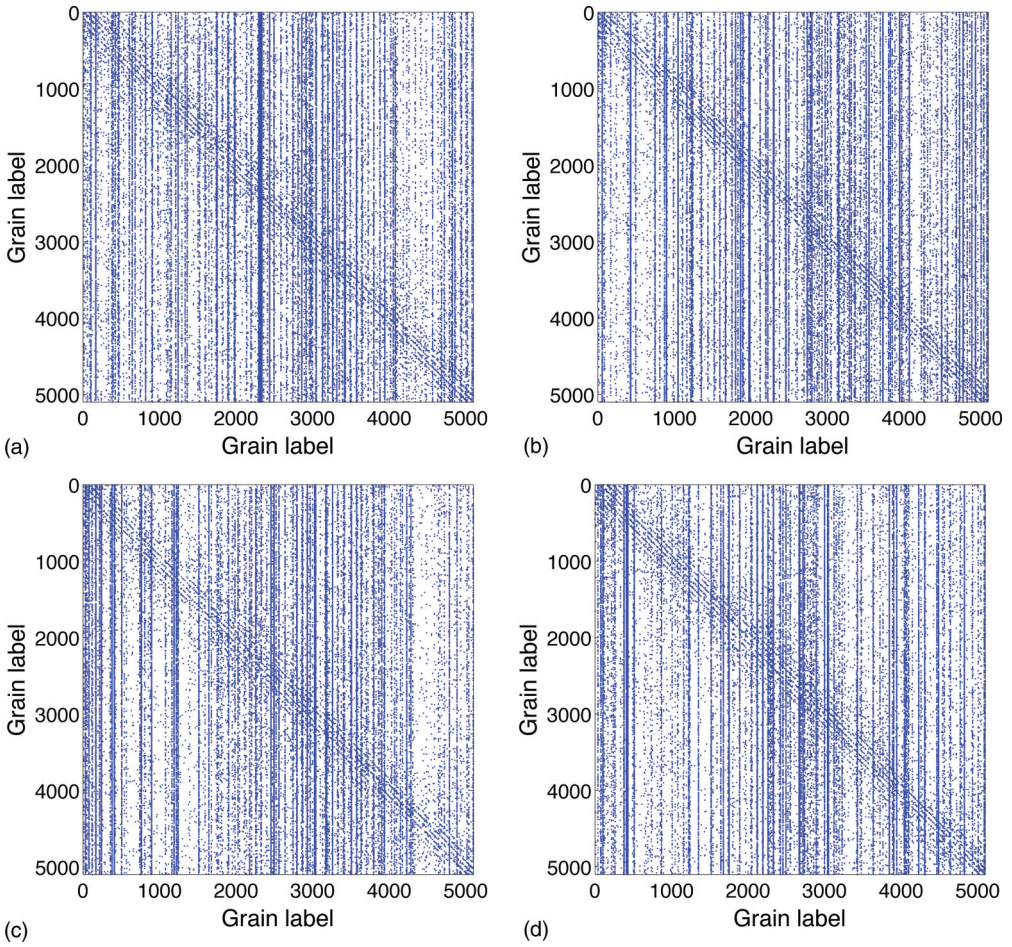

FIG. 5. (Color online) Adjacency matrices of the directed networks for each compression test. Constant confining pressure (a) $\mu^r = 0.02$, (b) $\mu^r = 0.2$. Constant volume (c) $\mu^r = 0.02$, (d) $\mu^r = 0.2$.

test systems. We also note that the power-law-like scatter of points quantifies the vertical lines present in the adjacency matrix plots, and highlights that some grains/sensors are present in many models of other grains. Similarly, there are a large population of grains/sensors whose particle load vector histories are rarely considered to be rich enough in information to participate in other grains' predictive model. If we recall the in-degree distribution, we actually find a few grains in all the tests that have a particle load vector history that is best predicted by a constant model; that is, no information from any other grain is deemed sufficient by description length to accurately model the history of any one of these few grains.

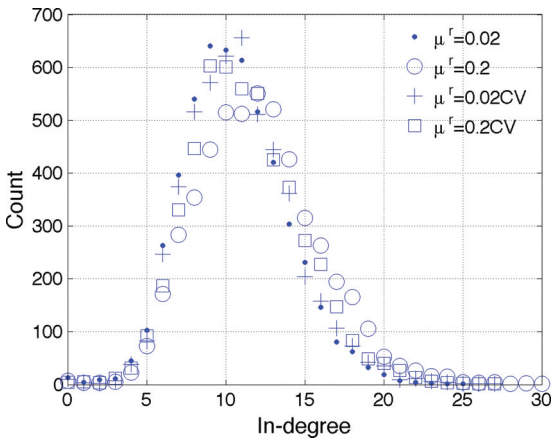

FIG. 6. (Color online) The empirical distributions of the in-degree of the reconstructed directed networks. Despite the different parameters, properties, and loading conditions for each test we see remarkable consistency in the in-degree distributions.

A. Spatial distribution

We have seen from the adjacency matrices and the in-degree and out-degree distributions that some grains are more important than others with respect to the number of models of other grains they appear in. An obvious question to ask is, where are these "smart" grains located? We consider the spatial location of grains which have an out-degree at least as high as their in-degree. That is, grains which appear in more models of other grains than the number of grains required to predict their own history. These are the grains corresponding to the vertical "lines" in Fig. 5. The number of grains which satisfy this directed network degree condition in each of the four tests is fairly steady: For the constant confining pressure tests, we have for $\mu^r = 0.02$ and 0.2, 379 and 282, respectively, whereas for the constant volume tests and $\mu^r = 0.02$ and 0.2 we find 287 and 302 smart grains, respectively. Thus, we can

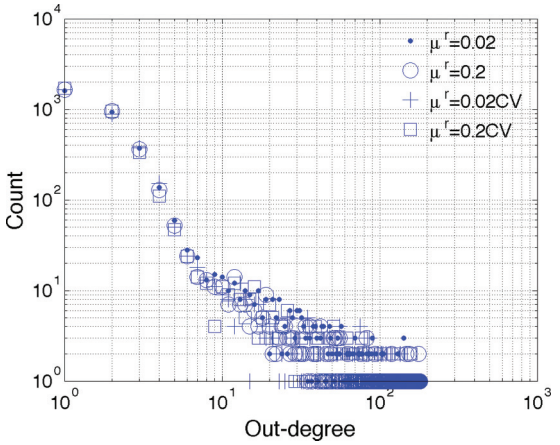

FIG. 7. (Color online) The empirical distributions of the out-degree of the reconstructed directed networks plotted on log-log scale. Once again we see remarkable consistency in the distributions across all four compression tests. We note that a straight line plot on this scale with or without cutoffs fails to satisfy a rigorous statistical significance test for the distribution to be adequately described by a power law.

modify the requirement of around 10 sensors to around 300 sensors in order to better track the representative behavior of the sample with respect to linear relationships of force interaction. Moreover, there are 56 common grains satisfying the above condition. The spatial location of all of these smart sensors and the sensors common to all four tests are shown in Fig. 8.

The smart grains/sensors appear to share other properties in common, both physical and functional. If we examine the grain size distribution of the smart sensors with respect to the polydisperse system we find that the smart sensors are typically smaller in size (see Fig. 9). A Kolmogorov-Smirnov test verifies that the difference in the smart grain size distribution and the size distribution of the remaining grains is statistically significant for all tests. In coarse-fine mixtures it is known that

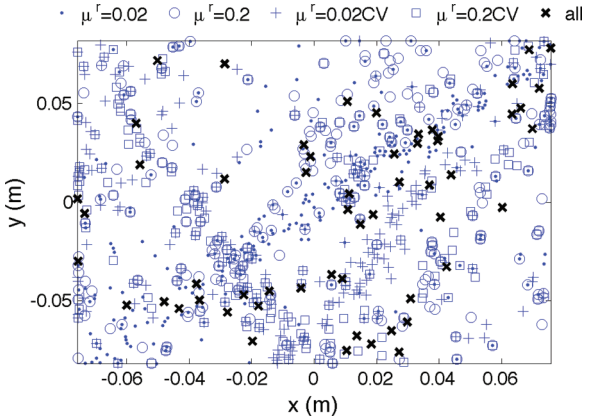

FIG. 8. (Color online) The spatial location of smart grains, i.e., grains which have at least a higher out-degree than in-degree in the constructed directed networks. Grain locations are plotted according to their position at the initial state of the samples for each test. The smart grains marked by crosses are those grains which are active for all four tests.

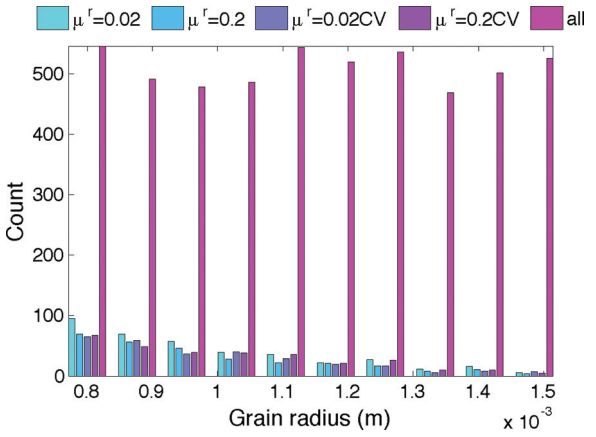

FIG. 9. (Color online) The grain size distribution of the smart grains in each test which have at least a higher out-degree than in-degree in the constructed directed networks compared to the size distribution of all grains. A KS test confirms that this difference in grain size distribution is statistically significant. Smart grains are typically smaller in size.

force chains tend to comprise the larger particles (e.g., [55,56]). We can examine the relationship of these smaller smart sensors with respect to their role in force chains. At each observed stage of the deformation history a grain can be classified as being a member of a force chain or not. A force chain is a quasilinear arrangement of three or more grains each possessing an above average particle load vector magnitude. For each smart sensor in each test we can determine whether they are classed as being part of a force chain or not and calculate the percentage of the deformation history when they are in force chains. In Fig. 10 we show the time of the deformation history each smart sensor spends as part of a force chain. Interestingly, in each test over half of the smart sensors are never classed as being a force chain particle: For the constant confining pressure tests, we have for $\mu^r = 0.02$ and 0.2, 50% and 54%, respectively, whereas for the constant volume tests and $\mu^r = 0.02$ and 0.2 we find 52% and 67% smart grains, respectively. This is consistent with observations of coarse-fine mixtures. Furthermore, even those smart sensors that are found to be in force chains typically do not spend a long time of the deformation history staying as force chains.

The smart sensors, however, do play an important role in force chain evolution, notably, force chain failure by buckling. In Fig. 11 for each of the four test systems we plot the spatial location of these grains, or smart sensors, represented by filled and unfilled black circles. Comparing with the kinematic displacement fields in Fig. 1, we find these grains reside in the regions of strain localization. It appears that the dynamics of grains in the shear band, as observed by their particle load vector time series history, is of the richest nature and essentially provides a basis or spanning set for the rest of the sample.

We have also overlaid these smart sensors on top of a density-like plot of grains which are involved in the physical mechanism of force chain buckling; i.e., the colored grains of Fig. 11 show every grain involved as either a 3-grain buckling segment of a force chain or a member of these segments' confining first ring of neighbors, so-called CBFCs (confined buckling of force chains) [34]. The color

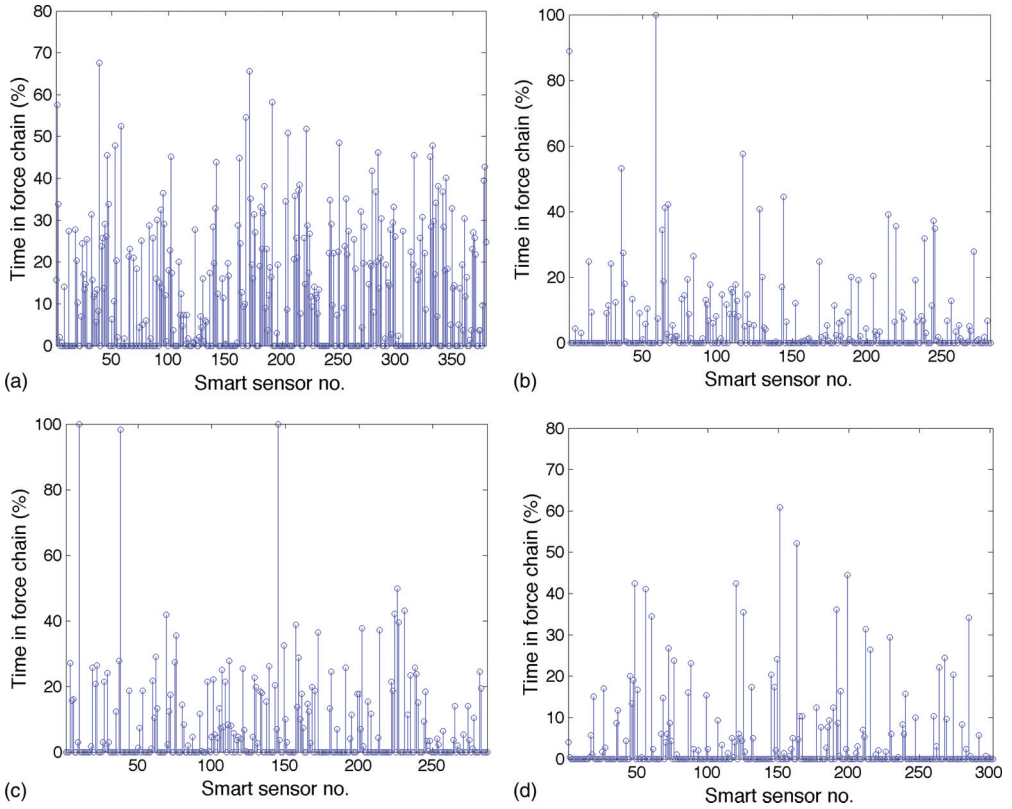

FIG. 10. (Color online) Constant confining pressure (a) $\mu^r = 0.02$, (b) $\mu^r = 0.2$. Constant volume (c) $\mu^r = 0.02$, (d) $\mu^r = 0.2$. The percentage of the deformation history when a smart sensor is a member of a force chain. In each test a large proportion of the smart sensors are *never* classed as a member of a force chain.

indicates the number of times a given grain is in one of these categories increasing from light to dark. The smart grains represented by the unfilled black circles coincide with this system failure mechanism of force chain buckling. The figures quoted below the plots indicate the relative makeup of the smart sensor (SS) and CBFC sets. We see that for the lower rolling friction tests, over half of the smart sensors are intimately related to the mechanism of force chain buckling and failure within dense granular materials. This discovery that a few appropriately placed sensors can be used to model the entire assembly has profound implications for the development of continuum theories. Our findings corroborate earlier findings that the nonlocal interactions—specifically germane to shear banding—are what governs force transmission and the related aspect of energy storage and dissipation in quasistatically deforming densely packed granular materials [27–29,34,37,57].

A remaining question is what mechanism or role do the other smart sensors (filled black circles) not involved in force chain buckling play within the material? In addition, why are other grains selected as useful according to the information fitting criterion for improved RAR modeling, even though they have not been classed as smart sensors (i.e., in-degree is higher than their network out-degree)? In order to distinguish these grains from SS grains, we refer to them as TS grains.

The TS grains are responsible for the diagonal-like lines in the adjacency matrix representations of Fig. 5 and their inclusion in the best RAR models can be attributed to proximity. These TS grains appear necessary in the RAR models, as they have local information of the stresses on grains throughout deformation. We can demonstrate our reason for this assertion by considering (with respect to the initial packing) the distribution over all grains of the distance between a grain and the grains in the best RAR model (i.e., a grain and those grains responsible for its in-links in the directed network). Furthermore, we can partition these distributions into contributions from the smart (SS) and other (TS) sensors. Figure 12 show these distributions for each test. Observe that the TS classed grains are typically distributed closer to the grains whose behavior they help predict and for each pair of distributions in all four tests a Kolmogorov-Smirnov test shows that a significant difference in the SS and TS distance distributions exists.

The set of smart sensor grains which are not directly associated with force chain buckling (filled black circles in Fig. 11) can also have their selection in most models as being due to proximity. However, there is another more intriguing explanation for their selection which gives a new perspective to considerations of microscopic and mesoscopic mechanisms crucial for robust predictions from continuum model formalisms. In [58], it was shown that the statistical properties of structural building blocks of planar granular materials—referred to as quadrons—are unduly influenced by the presence of so-called rattlers within the assembly. Rattlers are grains within the assembly that, for a period of the

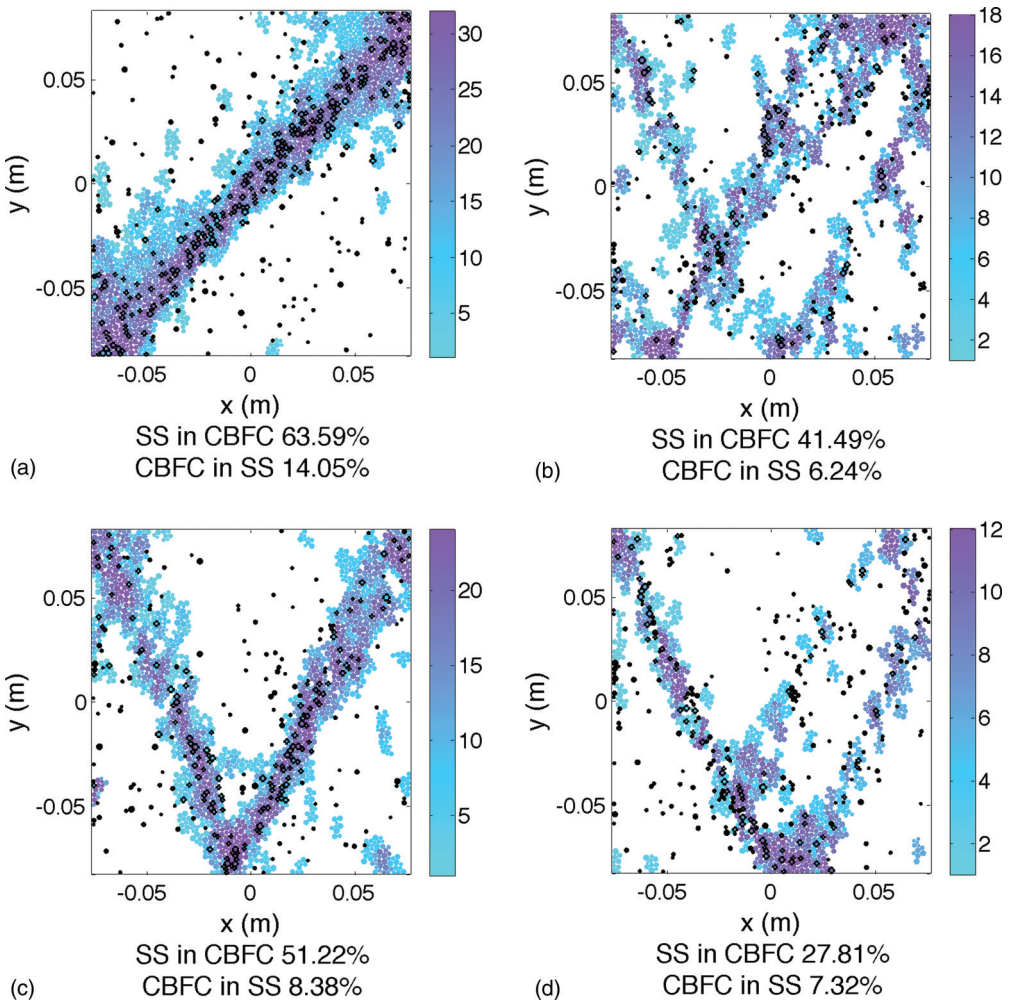

FIG. 11. (Color online) Constant confining pressure (a) $\mu^r = 0.02$, (b) $\mu^r = 0.2$. Constant volume (c) $\mu^r = 0.02$, (d) $\mu^r = 0.2$. A representation of the test assemblies at the initial stage of loading where black circles (unfilled) represent smart sensor (SS) grains in CBFCs and (filled) represent SS grains not associated with CBFCs. Smart sensor grains indicate a positive difference in the out- versus in-degree of the directed networks. The colored grains indicate a "density" plot of a grain's participation in the confined buckling of force chains through deformation. A comparison with the displacement fields of Fig. 1 reveals that the (unfilled) smart sensor grains and CBFC grains reside in the area of strain localization, i.e., the shear band. The percentages indicate that SS grains with the richest information regarding evolution of stress within the material predominantly reside in the area of richest kinematics.

deformation, have no or at most one contact and are thus unable to support significant stresses during this period. In the present context we define a rattler to be those grains whose nodes in an induced contact network—nodes are grains and links exist if the grains are in physical contact [40]—have node degree equal to zero. For example, see the time series trace in Fig. 3(c) which shows the number of contacts of grain ID 7 in the cluster of Fig. 3. In real systems, these rattlers sit snugly in a cavity inside the pore space of the assembly; when the material is deformed (e.g., sheared), the pore space gets squashed and suddenly the rattler becomes load bearing, and possibly even a member of a force chain in the next observation time step. For example, in Fig. 3, grain ID 7 spends 80% of its time as a rattler during the first half of the loading history, only changing its status to a nonrattler for a brief period to be involved in supporting the force chain before its failure through buckling. Furthermore, the mechanism of force chain buckling gives rise to open pores between the force chain and its confining neighbors. When a force chain collapses by buckling, so does the pore and the ensuing grain rearrangements in this unjamming event often involves intermittent rattlers. Could the smart sensors not associated with CBFC mechanisms be involved in this rattler mechanism? To identify whether this is indeed the case, we consider the distribution of times the smart sensors in CBFCs spend as a rattler throughout deformation and the time the smart sensors *not* in CBFCs spend as a rattler. In Fig. 13, we show these distributions for all four tests. In all cases, we see that the SS grains *not* in CBFCs spend a significantly longer time of the deformation history as a rattler, and so it appears that in addition to proximity these grains are included as important contributors to the RAR models because they are capturing the intermittent behavior of the status of the important mechanistic role rattlers play in the deformation of dense granular materials.

The importance of rattlers is often downplayed when explanations for the mechanisms behind granular failure are

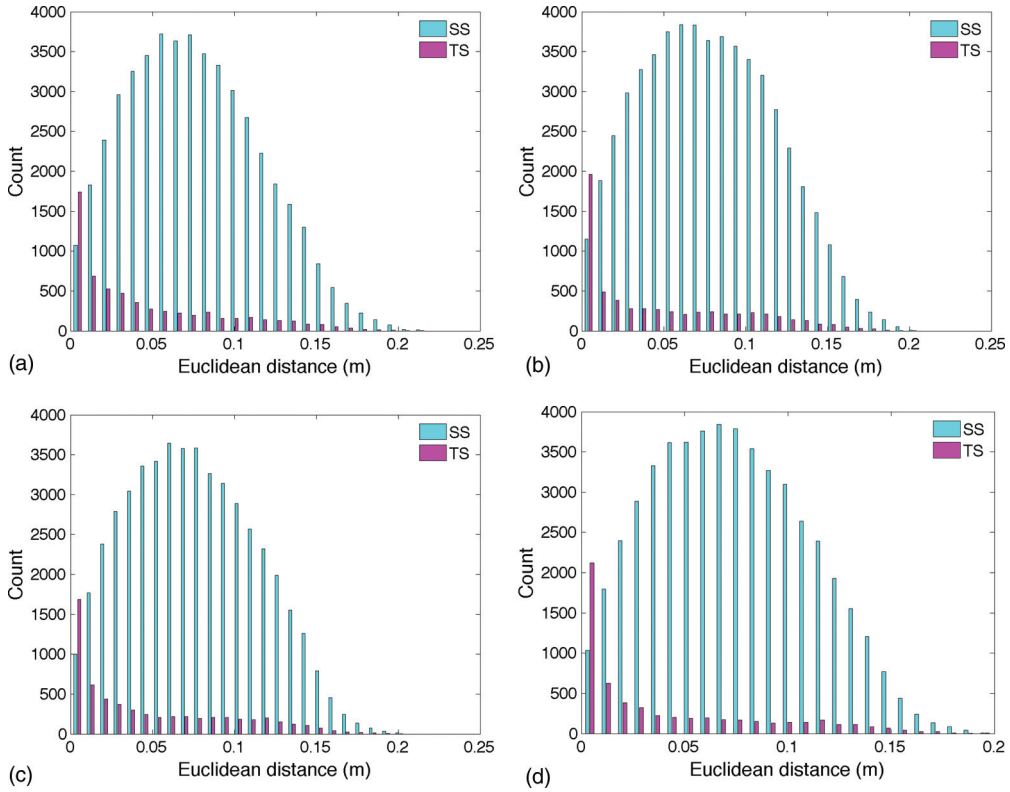

FIG. 12. (Color online) Constant confining pressure (a) $\mu^r = 0.02$, (b) $\mu^r = 0.2$. Constant volume (c) $\mu^r = 0.02$, (d) $\mu^r = 0.2$. The empirical distributions of the distances (with respect to the initial packing) of a grain and the other grains selected in the best RAR model of its stress response throughout deformation (i.e., those grains responsible for the in-links of a grain). The distribution is partitioned into two classes: the smart sensors (SS) and the other grains (TS). TS grains are typically closer to the grain being predicted and so their inclusion in the best RAR can be attributed to proximity and the local information they contain.

sought [59]. A reason for this is the quasistatic nature of compression tests and analysis. At any stage of the deformation rattlers are present but because, by definition, they have no load-bearing contacts these grains at a particular stage do not contribute to the determination of mechanical stiffness measures from stiffness matrices [59]. Moreover, since rattlers are present at all stages of deformation and their population does not significantly vary throughout deformation, the rattlers are often justifiably disregarded. What is ignored, however, is the temporal perspective and despite the overall cardinality of the set of rattlers being steady the membership of this set changes. We showed one example earlier of the intermittent status of a rattler throughout deformation in Fig. 3(c). This grain changed its status from a rattler to a load-bearing nonrattler precisely over the strain interval where a load-bearing force chain failed due to buckling. Thus, in addition to the correct treatment of rattlers in calculation of statistical measures being of import [58] their mechanistic role when they change their latent rattler status to one of active load-bearing should perhaps be reconsidered.

V. DISCUSSION

We have considered the possibility of the future design of grain sensors (gMEMs) and ways to turn information harvested from them to useful knowledge and tractable continuum models that can deliver robust predictions of granular behavior. To all intents and purposes, this sensor may exhibit the same rheological response as the material grains it is "sensing" but has the capabilities of modern microelectromechanical sensors to record and transmit detailed information of its surroundings. We posited that a useful granular sensor might be one which can sense its own internal stresses throughout loading. Restricting our study to the virtual, we considered the time series of grain stresses represented by a grain's particle load vector magnitude within a suite of DEM tests. Using a combination of information theory arguments, nonlinear time series modeling, and complex network methods, we showed that the observed stress behavior of a given grain in the assembly can be predicted based on information from a very few other grains. These few grains also exhibited the richest rheology in the system. We also observed that such apparently rich or smart grains resided in the areas of strain localization and were strongly linked to the governing failure mechanism of force chain buckling. Those smart grains not associated with force chain buckling appeared to spend a significant proportion of the loading history with the status of being a rattler, thus providing compelling additional evidence to the findings of [58] that the appropriate consideration of rattler behavior is key to a complete and thorough understanding of granular rheology. These findings were generic across the four different compressions tests.

The discovery that only a small number of sensors, placed in the locality of the shear band, is required to accurately

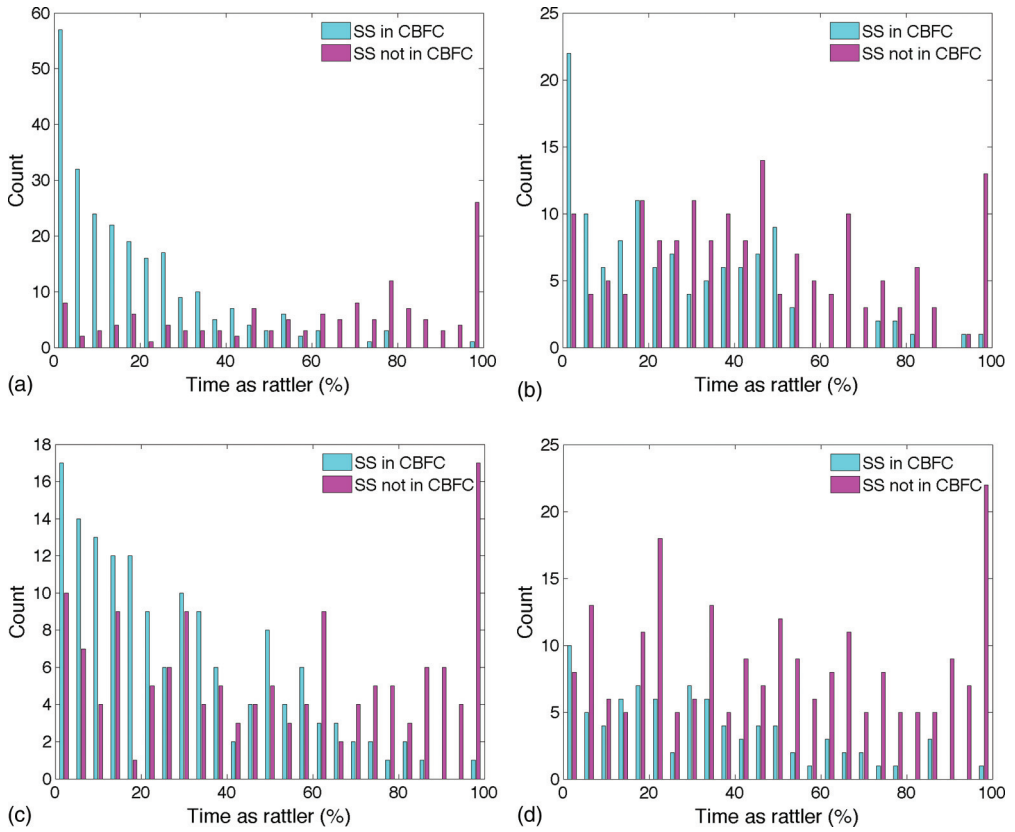

FIG. 13. (Color online) Constant confining pressure (a) $\mu^r = 0.02$, (b) $\mu^r = 0.2$. Constant volume (c) $\mu^r = 0.02$, (d) $\mu^r = 0.2$. The empirical distributions of the proportion of the deformation history the SS grains in and not in CBFC events spend as rattlers. The SS grains not part of CBFC events can be seen to be rattlers for a considerably longer period of the deformation history than the SS grains directly associated with CBFC events. Thus a second mechanism to perhaps consider in a continuum modeling formalism is the important role of rattler "dynamics".

capture the rheological response of all other grains highlights the crucial importance of nonlocal interactions, espoused by extended continuum theories which posit nonlocal evolution laws (e.g., [60–63]). This is especially the case with respect to the evolution of force chains, in particular, their failure by buckling. The relevance of nonlocal effects in dense granular materials, particularly in relation to force chain buckling, has been discussed in [64] and then incorporated into a nonlocal thermomicromechanical continuum model of Cosserat type in [34,39]. Our findings not only serve as a reminder that future advances in nonlocal continuum theory necessitate a multiscale approach, but also cast the spotlight on which microscopic and mesoscopic mechanisms, i.e., rattler behavior and force chain buckling, need to be addressed for robust predictions of deforming granular materials under compression and shear.

ACKNOWLEDGMENTS

We thank the anonymous referees for insightful comments and thought-provoking suggestions which helped improve the manuscript. This work was supported by US Army Research Office (W911NF-11-1-0175), the Australian Research Council (DP0986876), ARC Discovery Projects 2012 (DP120104759), and the Melbourne Energy Institute (A.T., D.M.W.). T.T. would like to acknowledge the support of a Grant-in-Aid for Scientific Research (C) (No. 24540419) from the Japan Society for the Promotion of Science (JSPS).

[1] MEMSnet, An Information Portal for the MEMS and Nanotechnology Community, https://www.memsnet.org/news.
[2] K. Terzaghi, Eng. News Record **85**, 632 (1920).
[3] L. Vu-Quoc, X. Zhang, and O. R. Walton, Comput. Methods Appl. Mech. Eng. **187**, 483 (2000).
[4] A. Dziugyz and D. Peters, Granular Matter **3**, 231 (2001).
[5] J. Zhang, T. S. Majmudar, A. Tordesillas, and R. P. Behringer, Granular Matter **12**, 159 (2010).
[6] A. L. Rechenmacher, S. Abedi, and O. Chupin, Geotechnique **60**, 343 (2010).
[7] S. A. Hall, M. Bornert, J. Desrues, Y. Pannier, N. Lenoir, G. Viggiani, and P. Bésuelle, Geotechnique **60**, 315 (2010).
[8] E. Andò, S. A. Hall, G. Viggiani, J. Desrues, and P. Bésuelle, Acta Geotechnica **7**, 1 (2012).
[9] N. W. Haymam, L. Ducloué, K. L. Foco, and K. E. Daniels, Pure Appl. Geophys. **168**, 2239 (2011).
[10] P. Guo, Acta Geotechnica **7**, 41 (2012).
[11] G. W. Hunt and J. Hammond, Philos. Mag. **92**, 3501 (2012).
[12] J. Paavilainen and J. Tuhkuri, Cold Reg. Sci. Technol. **85**, 157 (2013).

[13] A. Ord and B. E. Hobbs, Philos. Trans. R. Soc. A **368**, 95 (2010).
[14] K. Maeda, H. Sakai, A. Kondo, T. Yamaguchi, M. Fukuma, and E. Nukudani, Granular Matter **12**, 499 (2010).
[15] X. Zheng and D. Wang, Acta Mechanica Solida Sinica **23**, 579 (2010).
[16] D. R. Lester, M. Rudman, and P. J. Scales, Chem. Eng. Sci. **65**, 6362 (2010).
[17] D. Weaire, Curr. Opin. Colloid Interface Sci. **13**, 171 (2008).
[18] P. Coussot, Soft Matter **3**, 528 (2007).
[19] P. Rognon and C. Gay, Eur. Phys. J. E **30**, 291 (2009).
[20] K. D. Danov, P. A. Kralchevsky, and S. D. Stoyanov, Langmuir **26**, 143 (2010).
[21] B. Sandnes, E. G. Flekkoy, H. A. Knudsen, K. J. Maloy, and H. See, Nat. Commun. **2**, 288 (2011).
[22] M. Oda and H. Kazama, Geotechnique **48**, 465 (1998).
[23] M. Oda, T. Takemura, and M. Takahashi, Geotechnique **55**, 333 (2005).
[24] A. L. Rechenmacher, S. Abedi, and I. Faoro, in *Multiscale and Multiphysics Processes in Geomechanics*, edited by E. K. R. I. Borja, E. M. Dunham, and J. White (Springer, Stanford, 2010).
[25] A. Hasan and K. A. Alshibli, Geotechnique **60**, 369 (2010).
[26] A. L. Rechenmacher, S. Abedi, and O. Chupin, Acta Geotechnica **6**, 205 (2010).
[27] A. L. Rechenmacher, J. Mech. Phys. Solids **54**, 22 (2006).
[28] D. M. Walker, A. Tordesillas, S. Pucilowski, Q. Lin, A. L. Rechenmacher, and S. Abedi, Int. J. Bifurcation Chaos Appl. Sci. Eng. **22**, 1230042 (2012).
[29] M. Oda and K. Iwashita, Int. J. Eng. Sci. **38**, 1713 (2000).
[30] A. Tordesillas, S. Pucilowski, D. M. Walker, J. Peters, and M. Hopkins, Dynamics of Continuous, Discrete, and Impulsive Systems, Series B **19**, 471 (2012).
[31] A. Tordesillas, S. Pucilowski, L. Sibille, F. Nicot, and F. Darve, Philos. Mag. **92**, 4547 (2012).
[32] M. Muthuswamy and A. Tordesillas, J. Stat. Mech.: Theory Exp. (2006) P09003.
[33] A. Tordesillas, Philos. Mag. **87**, 4987 (2007).
[34] A. Tordesillas and M. Muthuswamy, J. Mech. Phys. Solids **57**, 706 (2009).
[35] Y. Guo and J. K. Morgan, J. Geophys. Res.: Solid Earth **109**, 1 (2004).
[36] P. A. Cundall and O. D. L. Strack, Geotechnique **29**, 47 (1979).
[37] A. Taboada, K.-J. Chang, F. Radjai, and F. Bouchette, J. Geophys. Res.: Solid Earth **110**, 1 (2005).
[38] A. Tordesillas, M. Muthuswamy, and S. D. C. Walsh, J. Eng. Mech. ASCE **134**, 1095 (2008).
[39] A. Tordesillas and M. Muthuswamy, Acta Geotechnica **3**, 225 (2008).
[40] D. M. Walker and A. Tordesillas, Int. J. Solids Struct. **47**, 624 (2010).
[41] A. Tordesillas, D. M. Walker, and Q. Lin, Phys. Rev. E **81**, 011302 (2010).
[42] A. Tordesillas, P. O'Sullivan, D. M. Walker, and Paramitha, C. R. Mec. **338**, 556 (2010).
[43] D. M. Walker and A. Tordesillas, Phys. Rev. E **85**, 011304 (2012).
[44] G. W. Hunt, A. Tordesillas, S. C. Green, and J. Shi, Philos. Trans. R. Soc. A **368**, 249 (2010).
[45] M. Small and K. Judd, Phys. Rev. E **59**, 1379 (1999).
[46] K. Judd and A. I. Mees, Physica D **82**, 426 (1995).
[47] M. Small, *Applied Nonlinear Time Series Analysis: Applications in Physics, Physiology, and Finance* (World Scientific, Singapore, 2005).
[48] T. Nakamura and T. Tanizawa, Physica A **391**, 4704 (2012).
[49] T. Tanizawa and T. Nakamura, in *2011 International Symposium on Nonlinear Theory and its Applications* (NOLTA2011, Kobe, Japan, 2011), pp. 690–692.
[50] K. Judd and A. I. Mees, Physica D **120**, 273 (1998).
[51] J. Zhang and M. Small, Phys. Rev. Lett. **96**, 238701 (2006).
[52] X. Xu, J. Zhang, and M. Small, Proc. Natl. Acad. Sci. USA **105**, 19601 (2008).
[53] Z. Gao and N. Jin, Chaos **19**, 033137 (2009).
[54] L. Lacasa, B. Luque, F. Ballesteros, J. Luque, and J. C. Nuno, Proc. Natl. Acad. Sci. USA **105**, 4972 (2008).
[55] C. Voivret, F. Radjai, J.-Y. Delenne, and M. S. El Youssoufi, Phys. Rev. Lett. **102**, 178001 (2009).
[56] J. F. Peters and E. S. Berney, J. Geotech. Geoenviron. Eng. **136**, 310 (2010).
[57] F. Alonso-Marroquin, I. Vardoulakis, H. J. Herrmann, D. Weatherley, and P. Mora, Phys. Rev. E **74**, 031306 (2006).
[58] T. Matsushima and R. Blumenfeld, arXiv:1207.2988 [cond-mat.soft].
[59] P. R. Welker and S. C. McNamara, Phys. Rev. E **79**, 061305 (2009).
[60] Z. P. Bažant and M. Jirásek, J. Eng. Mech. **128**, 1119 (2002).
[61] R. de Borst and L. J. Sluys, Comput. Methods Appl. Mech. Eng. **90**, 805 (1991).
[62] H. B. Muhlhaus and I. Vardoulakis, Geotechnique **37**, 271 (1987).
[63] A. Tordesillas, J. Shi, and J. F. Peters, Granular Matter **14**, 295 (2012).
[64] S. D. C. Walsh, A. Tordesillas, and J. F. Peters, Granular Matter **9**, 337 (2007).